

Study on temperature field and residual stress in T welding joint of stainless steel

Nguyen Tien Duong*

*School of Mechanical Engineering, Hanoi University of Science and Technology,
1 Dai Co Viet Street, Hai Ba Trung District, Ha Noi, Viet Nam*

*Emails: duong.nguyentien@hust.edu.vn

Received: 1 June 2023; Accepted for publication: 6 October 2024

Abstract. Stainless steels are increasingly used in the construction and transport sectors because they combine favorable aesthetic aspects, good mechanical properties and corrosion resistance. Hence, stainless steel structures have a long life with low maintenance costs. Local heating and cooling during welding produce a non-uniform temperature distribution. Uneven shrinkage of the welded joint creates residual stress in welded structures. This paper studies the temperature field during welding and the residual stresses after welding in T welding joint of stainless steel by the imaginary force method and the finite element analysis. The two plates in T-joint are thin plates. The two welds on either side of the T-joint are welded simultaneously using the MIG welding process. In this study, ESI SYSWELD finite element software is applied for thermo-mechanical analysis of stainless steel T welding joint. The residual stresses of this welding joint are calculated by the theory based on the imaginary force method. The results of temperature field and residual stresses in the T-joint are presented and discussed. The residual stress results determined by the finite element method are compared with the residual stress results calculated by the imaginary force method.

Keywords: Finite element analysis, imaginary force method, residual stress, stainless steel, T-joint.

Classification numbers: 5.1.1, 5.1.4.

1. INTRODUCTION

Stainless steel has been used in construction for over one hundred years. Stainless steel structures are corrosion resistant with low maintenance requirements. They have good strength, toughness and fatigue properties. Welding is used to fabricate many steel structures. The metal inert gas (MIG) welding process is widely employed in order to weld stainless steel. This welding process gives high productivity and quality. Uneven cooling and heating in the joint are the major cause of residual stresses in welded structures.

Four methods are commonly used to calculate the welding residual stresses [1]: imaginary force method (IFM) [2], elasticity theory [3], general theory of welding deformations and stresses [4], and numerical method. The imaginary force method gives the coarse approximation of the solution but it satisfies the requirements of industries because of fast calculation. The

numerical method includes finite element method, finite difference method, boundary element method, etc.

The finite element method (FEM) has become a key technology in the modeling and simulation of engineering systems in different sectors such as building, transportation, communications, etc. There are many studies on the temperature field and residual stress in welding carbon steel in general and stainless steel in particular using the finite element method. Raffaele Sepe *et al.* [5] used ABAQUS software which is based on the finite element method to study the temperature field and residual stress in two-pass V-groove butt weld joint of S275JR structural low carbon steel. In their study, the temperature field during welding and the deformation after welding obtained by the numerical method are compared with an experimental test on the specimen. Dhayanithi Venkatkumar and Durairaj Ravindran [6] studied the effect of boundary conditions on the residual stresses and strain of 316 stainless steel butt weld joints using ANSYS finite element software. Chong Yi Wei and WenGuang Jiang [7] investigated residual stresses in T-joint of DH36 carbon steel by applying ANSYS language code. The finite element software packages such as NASTRAN, MARC, ABAQUS, ANSYS, SYSWELD, etc. [5-8] can be used for welding residual stress analyses. SYSWELD is a special-purpose finite element analysis software applied to heat treatment and welding processes [9].

In this study, firstly, the imaginary force method is applied to calculate the residual stresses in stainless steel T-joint of thin plates. In arc welding, the limited thickness of thin plates is 20 mm [2]. Then SYSWELD finite element software is used to determine the temperature field and residual stresses of this joint. Two weld seams on both sides of the T-joint are performed at the same time. These welds are made using the MIG welding process.

2. RESIDUAL STRESS DETERMINATION BY IMAGINARY FORCE METHOD

This section is based on the imaginary force method [2] to develop a formula for determining the welding residual stress of the T-joint.

2.1. Longitudinal stress of T-joint due to vertical contraction

The active stress zone (crossed area in Figure 1) is determined by following formula:

$$F_{ac} = F_{ac1} + F_{ac2} + F_w \quad (1)$$

in which: F_{ac1} is the active stress zone in flange: $F_{ac1} = (2 \cdot b_{n1} + \delta_1) \cdot \delta_1$; b_{n1} is the active stress zone in each half flange: $b_{n1} = b_{11} + b_{21}$; F_{ac2} is the active stress zone in web: $F_{ac2} = b_{n2} \cdot \delta_2$; b_{n2} is the active stress zone in web: $b_{n2} = b_{12} + b_{22}$; F_w is the active stress zone in two welds: $F_w = K^2$ (K is the throat thickness of fillet weld).

b_{11} and b_{12} are the regions which have undergone the plastic deformation during welding. They are generally denoted b_1 . In the case of thin plate, this region is determined by the following formula [2]:

$$b_1 = \frac{0,484 \cdot q}{\sum \delta \cdot v \cdot c \cdot \rho \cdot T_m} \quad (2)$$

In this formula, T_m is the temperature of changing from plastic to elastic state of the material (called change temperature); $\sum \delta$ is the total thickness of heat transfer. In T-joint, it is:

$$\sum \delta = 2 \cdot \delta_1 + \delta_2 \quad (3)$$

b_{21} and b_{22} are the regions which have undergone the elastic state during welding. They are generally denoted b_2 [2]:

$$b_2 = k_2 \cdot (h_w - b_1) \quad (4)$$

in which: h_w is the calculated width, its value depends on the welding process; k_2 is the coefficient determined by the graph [2]. This coefficient depends on the specific energy of heat source (q_0) and the yield strength of material (σ_Y). The specific energy of heat source (q_0) is determined by equation:

$$q_0 = Q \cdot (v \cdot \Sigma \delta)^{-1}$$

where Q is the net power of welding heat source [10]: $Q = U \cdot I \cdot \eta$. In this equation, U is the welding potential; I is the welding current; η is the efficiency factor of welding arc; v is the welding speed.

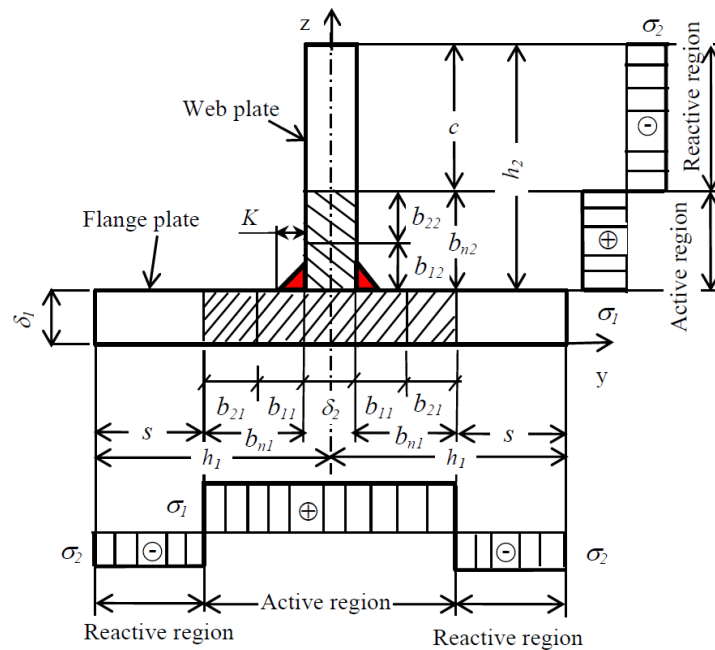


Figure 1. Cross section and stress regions of T welding joint.

The total active internal force of active stress zone is given by:

$$P = P_1 + P_2 + P_w \quad (5)$$

where: P_1 is the active internal force in flange, $P_1 = \sigma_{x-ac} \cdot F_{ac1}$; σ_{x-ac} is the active longitudinal stress and $\sigma_{x-ac} = \sigma_Y$ [2]; σ_Y is the yield strength of the base metal and also of the weld metal; P_2 is the active internal force in web, $P_2 = \sigma_{x-ac} \cdot F_{ac2}$; P_w is the active internal force in two welds, $P_w = \sigma_{x-ac} \cdot F_w$.

The total reactive internal force is determined by equation: $P' = \sigma_{x-re} \cdot F_{re}$.

where: σ_{x-re} is the reaction longitudinal stress; F_{re} is the reaction zone area, $F_{re} = 2 \cdot s \cdot \delta_1 + c \cdot \delta_2$.

In the above expression, s is the width of reaction zone at each half flange: $s = h_{1c} - b_{n1}$; c is the width of reaction zone at the web: $c = h_{2c} - b_{n2}$; where: h_{1c} and h_{2c} are the calculated width of

each half flange and of the web, respectively. If $h_{1c} > (h_1 - \delta_2/2)$ then it takes: $h_{1c} = (h_1 - \delta_2/2)$. If $h_{2c} > h_2$ then it takes: $h_{2c} = h_2$.

From balance condition of internal force ($P = P'$), it gives: $\sigma_{2x-re} \cdot F_{re} = P$. So, it leads to:

$$\sigma_{x-re} = P / F_{re} \quad (6)$$

2.2. Transverse stress of T-joint due to vertical contraction

The transverse stress at a point of a distance x from the beginning of the weld along the length of the active stress zone in the flange plate is determined by the following formula:

$$\sigma_y = \frac{16 \cdot \sigma_Y \cdot b \cdot n_1 \cdot h_1}{l^2} \left[\frac{6 \cdot x \cdot (l - x)}{l^2} - 1 \right] \quad (7)$$

where l is the length of T-joint.

3. SIMULATION OF T WELDED JOINT BY FINITE ELEMENT METHOD

The thermal analysis is performed to determine the temperature distributions in welded T-joint. The MIG welding is an arc welding process in which the thermal conduction through the welding body is the major type of heat transfer. The temperature field T at the point (x, y, z) and in the time t is determined by solving the heat transfer equation [8]:

$$K \left(\frac{\partial^2 T}{\partial x^2} + \frac{\partial^2 T}{\partial y^2} + \frac{\partial^2 T}{\partial z^2} \right) + q = \rho c \frac{\partial T}{\partial t} \quad (8)$$

in this equation, q is the volumetric heat flux; K , ρ , c are thermal conductivity, density and specific heat, respectively.

In this research, the welding is realized in double side of T-joint. A double semi-ellipsoidal heat source model proposed by Goldak and Akhlaghi [11, 12] is employed to simulate the MIG welding process. The torch angle relative to the flange plate is $\theta = 45^\circ$ for the right side weld and $\theta = -45^\circ$ for the left side weld of T-joint. In T-joint weld, a coordinate transformation is employed as shown in Figure 2. The front and rear heat source density distributions of the ellipsoid in the fillet welds of T-joint are described in Equation (9) and Equation (10), respectively [7, 11, 12]:

$$q_1(x, y, z) = \frac{6\sqrt{3}f_1Q}{a_1bc\pi\sqrt{\pi}} \exp\left(-\frac{3x'^2}{a_1^2} - \frac{3y'^2}{b^2} - \frac{3z'^2}{c^2}\right) \quad (9)$$

$$q_2(x, y, z) = \frac{6\sqrt{3}f_2Q}{a_2bc\pi\sqrt{\pi}} \exp\left(-\frac{3x'^2}{a_2^2} - \frac{3y'^2}{b^2} - \frac{3z'^2}{c^2}\right) \quad (10)$$

in which: $x' = (x - x_0 - vt)$; $y' = (y - y_0) \cos \alpha + (z - z_0) \sin \theta$; $z' = -(y - y_0) \sin \alpha + (z - z_0) \cos \theta$.

In the above formulas, (x_0, y_0, z_0) is the position of the point where the welding torch is aimed in the (x, y, z) coordinate system; f_1 and f_2 are the fraction of the deposited heat in the front

and the rear parts, in which: $f_1 = 2.a_1 / (a_1 + a_2)$ and $f_2 = 2.a_2 / (a_1 + a_2)$; a_1 , a_2 , b and c are the geometry characteristics of the heat source for MIG welding process.

The thermal history at each node in the weld joint is used to predict the residual stresses after welding. The obtained thermal history in the thermal analysis is used as temperature load in the mechanical analysis. The stress components are obtained by solving the three governing partial differential equations of force equilibrium. In tensor notation, they have the form:

$$\sigma_{ij,i} + p_j = 0 \quad (11)$$

where p_j is the body force and σ_{ij} is the stress tensor.

In the finite element formulation, these equilibrium equations are replaced with an equivalent “weak form”, the principle of virtual work is written as:

$$\int_V \sigma_{ij} \delta \bar{\epsilon}_{ij} dV = \int_V p_i \delta \bar{u}_i dV + \int_S T_i \delta \bar{u}_i dS \quad (12)$$

where $\delta \bar{\epsilon}$ is the virtual strain, $\delta \bar{u}$ is a virtual displacement field, T is the surface traction at any point on S .

When solving the equilibrium equations, the small strain theory is used in welding processes. The total strain (ϵ_{ij}^{total}) is calculated by the following formula:

$$\epsilon_{ij}^{total} = \epsilon_{ij}^e + \epsilon_{ij}^{pl} + \epsilon_{ij}^{th} \quad (13)$$

where ϵ_{ij}^e , ϵ_{ij}^{pl} and ϵ_{ij}^{th} are the elastic, plastic and thermal strain parts, respectively.

The relation between strains and displacements is given in matrix form:

$$\{\epsilon^{total}\} = [B]\{u\} \quad (14)$$

where $[B]$ is the fundamental strain-displacement matrix.

The stresses in a finite element are related to the element strains in terms of the actual constitutive law:

$$\{\sigma\} = [C]\{\epsilon^{total}\} \quad (15)$$

where $[C]$ is the constitutive matrix which is described by Hooke’s law for a thermo-elastic material.

Both thermal analysis and mechanical analysis are performed using the finite element method. In this work, the finite elements in 3 dimensions are developed. In order to increase the accuracy and to reduce the number of elements, a fine mesh is defined in regions near the weld seam and a coarser mesh is implemented in regions away from the weld seam.

4. NUMERICAL APPLICATION

The dimensions of flange plate are $200 \times 200 \times 10$ mm. The web plate has the dimensions of $200 \times 100 \times 10$ mm. The base material of the two plates and the deposited metal is AISI 316L stainless steel. The mechanical properties at room temperature of this material are presented in Table 1 [9, 13 - 15]. The melting point of this steel is 1450 °C [9].

Table 1. Mechanical properties of 316L stainless steel.

Property	Elastic modulus (GPa)	Yield strength, σ_y (MPa)	Tensile strength (MPa)	Elongation (%)	Poisson's ratio
Value	195	207	538	55	0.294

Two welds of single pass are performed simultaneously on both sides of the T-joint. The leg of the fillet weld is 6 mm. The dimensions of the T-joint are given in Figure 2.

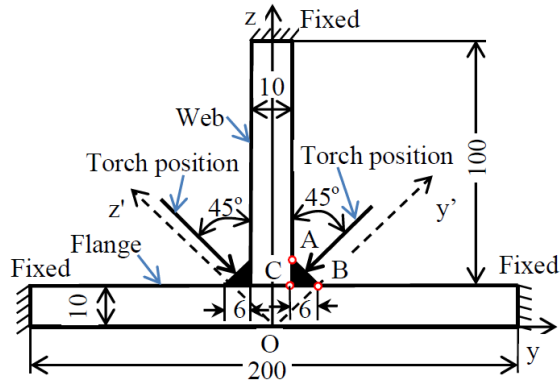


Figure 2. Dimensions of T welded joint and boundary condition in case 2.

The clamping condition of T-joint is considered in two cases: Case 1 - Free shrinkage (called “no clamp”) and Case 2 - Clamping at 3 outer side faces of two plates (called “clamp”). The boundary condition of case 1 is the fixation of the displacement component in Oy direction along the center line of flange plate bottom surface because of the symmetry of the structure and the welds. The welding parameters are: $I = 260$ A, $U = 28$ V, welding speed $v = 5$ mm/second, efficiency of heat input $\eta = 0.85$, torch angle $\theta = \pm 45^\circ$.

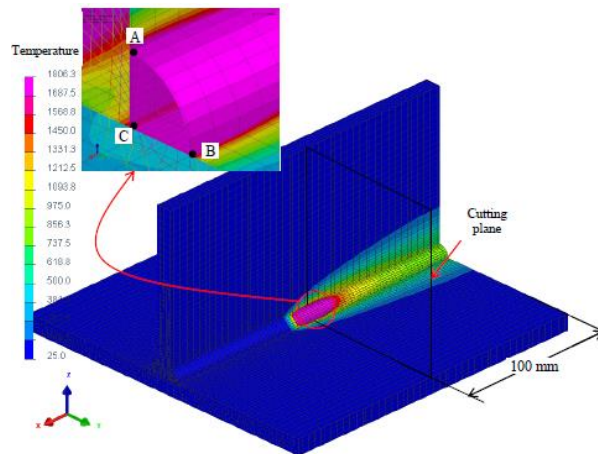


Figure 3. Finite element mesh, temperature field in T-joint and 3 investigated points.

The geometry parameters of heat source model are $a_f + a_r = 12$ mm, $b = 4.5$ mm, $c = 5.5$ mm, respectively to the length, width and penetration of the welding pool. SYSWELD software

based on the finite element method is used for thermal and mechanical analyses in this study. Eight-node 3D elements are implemented. The total number of nodes for the finite element model is 82535 nodes. The total number of elements for this model is 71484 elements. In the vicinity of the weld seam, a fine mesh is constructed. The smallest element has the dimensions of $0.375 \times 0.387 \times 2.38$ mm. The element dimensions increase with increasing distance from weld seam. The finite element mesh of T-joint is presented in Figure 3.

5. OBTAINED RESULTS AND DISCUSSION

5.1. Results of temperature field

The research results show that the welding temperature field with clamp and without clamp is the same. The temperature at 3 points belonging to the middle plane (cutting plane - Figure 3) of the weld path is considered: weld toe on the web plate (Point A), weld toe on the flange plate (Point B), and joint root (Point C) (Figure 2 and Figure 3). The temperature variation at these points as a function of the welding time is presented in Figure 4. The maximum temperature at points A and B is reached 21 seconds after starting welding. Point C obtains the maximum temperature 21.5 seconds after starting welding. It means that these points obtain the maximum temperature when the welding heat source has passed through the survey points a distance of 5-7.5 mm. The temperature at the survey points begins to increase rapidly when the welding heat source goes closer to these points. After the welding heat source passes through these points, the temperature at these points decreases very quickly. The maximum temperature at 3 points A, B and C is 1924.56 °C, 1880.95 °C and 1609.19 °C, respectively. The weld toes (on the web and on the flange) and the joint root are melted because the maximum temperatures at these points are above the melting point of the parent material (=1450 °C). The depth of fusion at the weld toes on the web plate and flange plate is 0.76 mm and 0.62 mm, respectively. The width of the heat-affected zone (HAZ) on the web plate and flange plate is 4.3 mm and 2.9 mm, respectively.

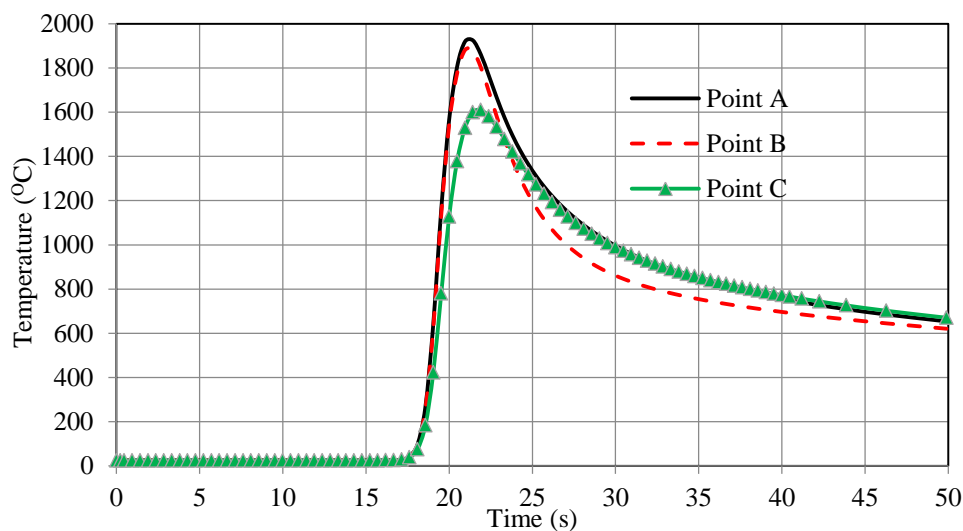


Figure 4. Temperature at 3 points as a function of welding time.

Figure 5 presents the temperature distribution along the horizontal path at the middle of the web plate and of the flange plate starting at the joint root when the center of the heat source is in

the middle of the weld line. The temperature at the weld center is the highest. It drops very quickly away from the weld center. The temperature of points with a distance of 20 mm or more from the weld center is almost unchanged. At any time during welding and also during cooling, the temperature of the point on the web plate is always higher than the temperature of the point on the flange plate that has the same distance to the joint root.

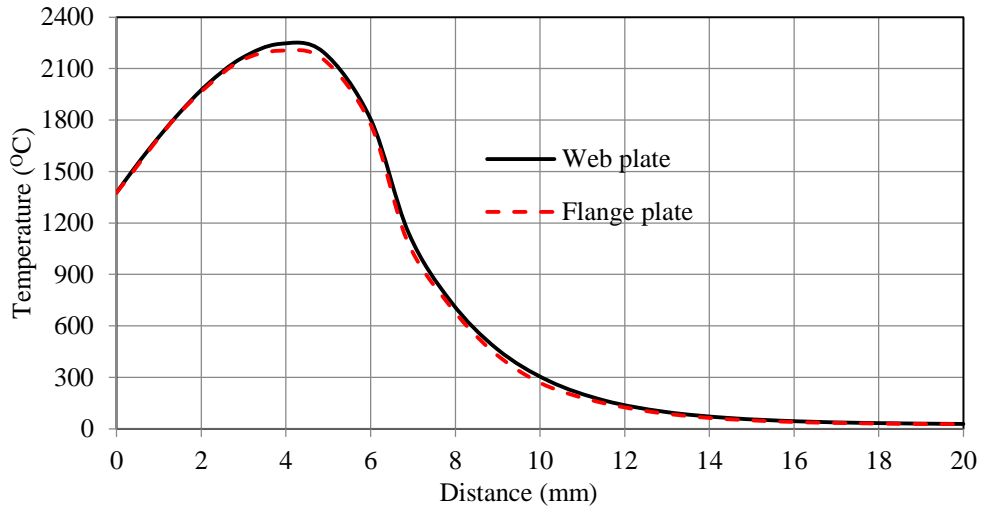


Figure 5. Temperature along the horizontal path.

5.2. Results of stress field

The longitudinal residual stress distribution along the vertical center path on the bottom face of the flange plate is given in Figure 6. At both ends of this path, the longitudinal stress is zero. It reaches its maximum value at the center of the path. The maximum longitudinal stress in case 1 (322 MPa) is 11.7 % greater than that in case 2 (284.2 MPa).

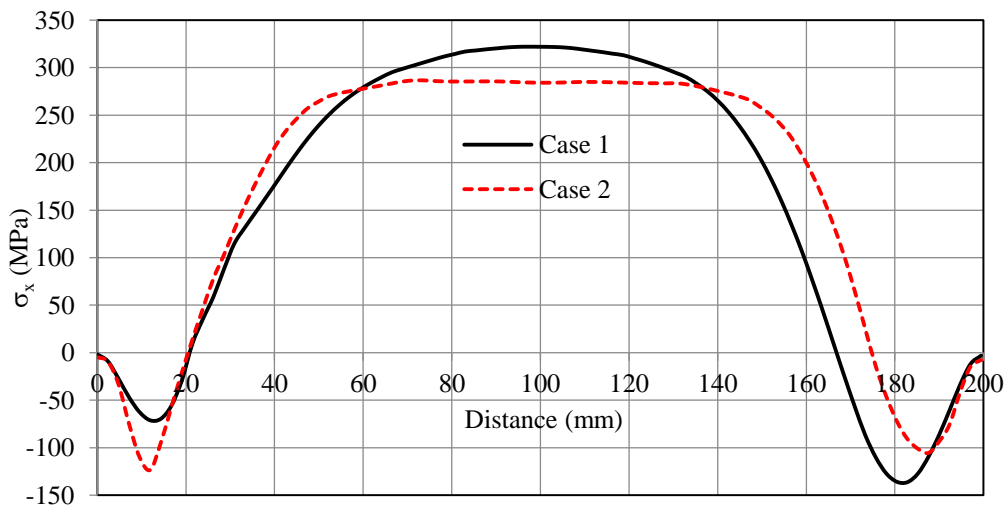


Figure 6. Longitudinal stress along the vertical center path of the flange.

In the next parts, the residual stress results obtained by the simulation of SYSWELD finite element software in two cases are compared with the residual stress results calculated by the imaginary force method (IFM). In the case of calculation using the imaginary force method, the boundary condition of the T-joint is free (no clamping) that is similar to case 1 in the finite element method. So the stress results in case 1 will be compared with the stress results of the imaginary force method.

Figure 7 indicates the transverse stress distribution along the vertical center path on the bottom face of the flange plate. This stress at both ends of this path is negative. It is positive in the middle of the path. The transverse stress distribution along the vertical center path on the bottom face of the flange plate is in agreement with the IFM: The transverse stress at both ends of the path is compressive stress; it is tensile in the middle of the path. The difference in the maximum tensile transverse stress at the midline between case 1 (184.03 MPa) and the IFM (165.6 MPa) is 10 %. The difference in the maximum compressive transverse stress at the weld seam end between case 1 (300.1 MPa) and the IFM (331.2 MPa) is 10.4 %. The maximum transverse stress in the center of the path in case 1 (184.03 MPa) is under the yield strength of the parent metal (= 207 MPa). This stress in case 2 (268.8 MPa) is higher than the yield strength of the parent metal. The maximum transverse stress in the case of clamp is 1.5 times greater than that in the case of no clamp. In the case of clamp on both outer edges of the flange plate (the case 2), the flange plate is not possible to shrink freely in the horizontal direction after welding. So the transverse residual stress is greatly increased.

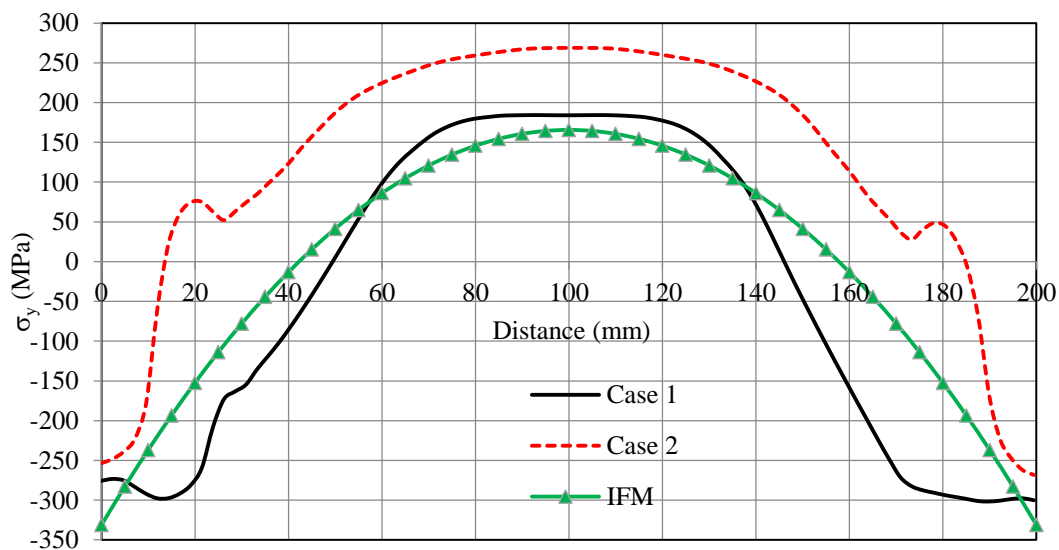


Figure 7. Transverse stress along the vertical center path of the flange.

The longitudinal stress distribution along the horizontal center path on the bottom face of the flange plate is presented in Figure 8. The longitudinal stress distribution along the horizontal center path on the bottom face of the flange plate in case 1 of the FEM is consistent with that of the IFM: The active longitudinal stress is tensile; the reactive longitudinal stress is compressive. The maximum active longitudinal stress in case 1 of the FEM (322 MPa) is 1.56 times larger than that of the IFM (207 MPa). The maximum reactive longitudinal stress in case 1 of the FEM (225.16 MPa) is 1.67 times greater than that of the IFM (134.87 MPa). The width of the active

stress zone on the flange plate in case 1 of the FEM (26.5 mm) is about 1.51 times smaller than that of the IFM (40 mm).

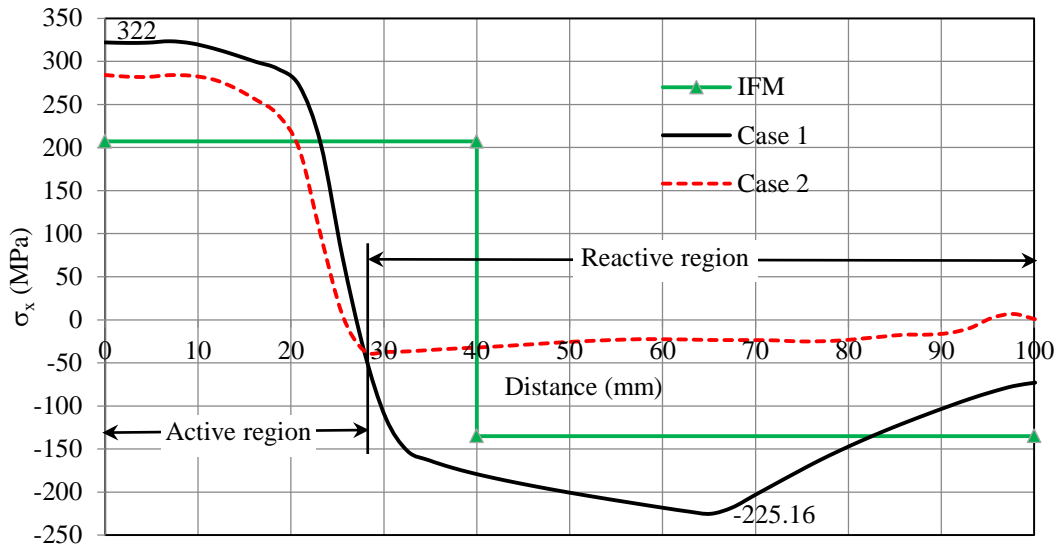


Figure 8. Longitudinal stress along the horizontal center path of the flange.

The active longitudinal stress in both cases is higher than the yield strength of the parent material. The maximum reactive longitudinal stress in the case of no clamp (225.2 MPa) is 6 times higher than that in the clamped case (37.2 MPa). The width of the active stress region on the flange plate in both cases is not significantly different (case 1 = 26.5 mm, case 2 = 25.6 mm). The longitudinal stress at the edge of the flange plate in the non-clamp case is quite large (72.9 MPa). It is close to zero in the clamped case.

Figure 9 shows the longitudinal stress distribution along the horizontal center path at the right face of the web plate.

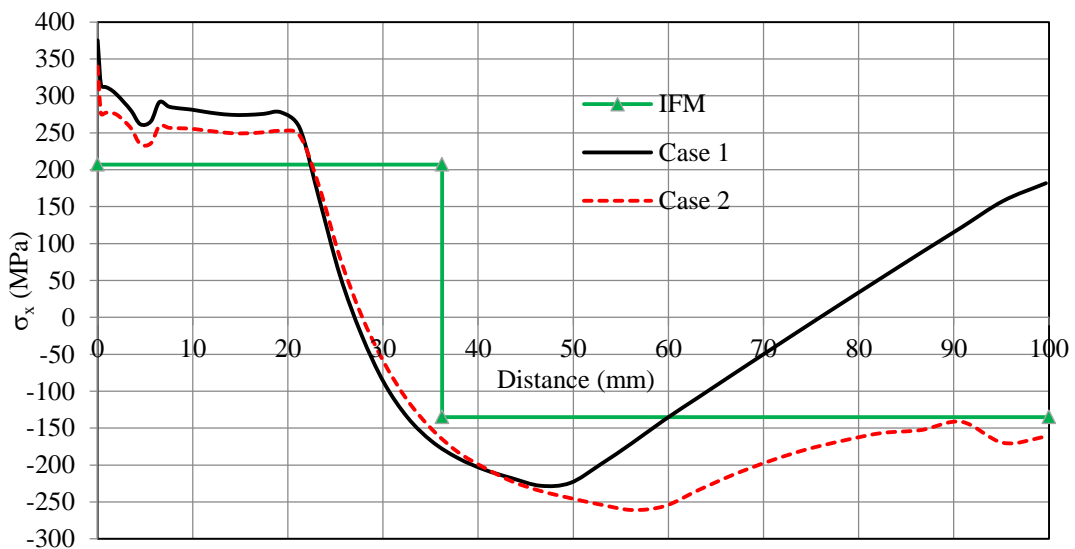


Figure 9. Longitudinal stress along the horizontal center path of the web.

The longitudinal stress distribution along the horizontal centerline at the right face of the web plate in case 2 of the FEM is suitable to that of the IFM: The longitudinal stress in the active region is tensile; it is compressive in the reactive region. In case 1, this stress in the active region is tensile; on the inside of the reactive region, it is compressive; but it is tensile in the region near the web plate edge. The maximum active longitudinal stress in case 1 of the FEM (281.5 MPa) is 1.36 times larger than that of the IFM (207 MPa). The maximum reactive longitudinal stress in case 1 of the FEM (228 MPa) is 69 % greater than that of the IFM (134.87 MPa). The reactive longitudinal stress at the edge of web plate in case 2 of the FEM (161.5 MPa) is 19.7 % larger than that of the IFM (134.87 MPa). The width of the active stress zone on the web plate in case 1 of the FEM (27 mm) is approximately 25.4 % smaller than that of the IFM (36.2 mm). In the active stress region, the maximum longitudinal stress in the non-clamp case (281.5 MPa) is 7.9 % greater than that in the case of clamp (259.2 MPa). In the reactive stress zone, the longitudinal stress in the clamped case (260.8 MPa) is 14.4 % higher than that in the non-clamp case (228 MPa). The longitudinal stress at the outer edge of the web plate in the non-clamp case (181.7 MPa) is the tensile stress. But it is the compressive stress in the case of clamp (-161.5 MPa). The width of the active stress region on the web plate in both cases is almost the same. It is 27 mm in the case 1 and 27.8 mm in the case 2.

6. CONCLUSIONS

The research results of stainless steel MIG welding on both sides at the same time of T-joint in two cases of free boundary conditions and of fixation at three outer edges show that:

- The temperature of a point on the weld seam only starts to increase when the welding heat source moves closer to that point. The temperature of a point on the web plate is always higher than the temperature of a point on the flange plate at the same distance to the joint root.

- The transverse stress on the vertical center line at the bottom face of the flange plate in the FEM is about 10 % greater than the transverse stress on the longitudinal line in the IFM. The longitudinal stress on the horizontal centerline at the bottom face of the flange plate in the FEM is about 1.6 times higher than that in the IFM.

- The transverse stress on the vertical center path of the flange plate in the clamped case is much higher than that in the non-clamp case. The maximum reactive longitudinal stress on the horizontal center path at the bottom face of the flange plate in the non-clamp case is 6 times higher than that in the clamped case. The longitudinal stress at the outer edge of the flange plate in the clamped case is zero. But it is quite large in the non-clamp case.

- The width of the active stress zone on the flange plate and on the web plate in the FEM is always smaller than that in the IFM. The longitudinal stress at the outer edge of the web plate in the case of no clamp is the tensile stress. It is the compressive stress in the case of clamp.

The IMF method does not accurately represent the stress at each point in the action and reaction regions. The results of the FEM method show that this stress varies from point to point in each region. However, the IFM method gives fast calculation results. This method can be used for preliminary calculation of welding stress.

CRedit authorship contribution statement. Author Nguyen Tien Duong: Entire content of this paper.

Declaration of competing interest. The author declares that he has no known competing financial interests or personal relationships that could have appeared to influence the work reported in this paper.

REFERENCES

1. Nguyen Tien Duong - Determination of welding deformations of I beam by the general theory of welding deformations and stresses, *Journal of Science and Technology - Technical universities* **106B** (2015) 1-6.
2. Trochun I. P. - Internal forces and deformations during welding, State Scientific and Technical Publishing House of Machine-Building Literature, Moscow, 1964 (in Russian).
3. Vasil'ev V. I. - Deformation of structural units due to transverse welds (*Deformatsii elementov konstruksii ot poperechnykh svarnykh shvov*), LKI, 1954.
4. Okerblom N. O. - The calculations of deformations of welded metal structures, Department of Scientific and Industrial research, London, Her Majesty's stationery Office, 1958.
5. Raffaele Sepe, Alessandro De Luca, Alessandro Greco, Enrico Armentani - Numerical evaluation of temperature fields and residual stresses in butt weld joints and comparison with experimental measurements, *Fatigue & Fracture of Engineering Materials & Structures* **44** (2021) 182-198.
6. Dhayanithi Venkatkumar, Durairaj Ravindran - Effect of boundary conditions on residual stresses and distortion in 316 stainless steel butt welded plate, *High Temperature Materials and Processes* **38** (2019) 827-836.
7. Chong Yi Wei, WenGuang Jiang - Influence of welding groove on residual stress and distortion in T-joint weld, *International Conference on Novel Functional Materials, IOP Conference Series: Materials Science and Engineering* **733** (2020) 012010, doi:10.1088/1757-899X/733/1/012010
8. Lee S. H., Kim E. S., Park J. Y., Choi J. - Numerical analysis of thermal deformation and residual stress in automotive muffler by MIG welding, *Journal of Computational Design and Engineering* **5** (2018) 382-390.
9. Nguyen Tien Duong - Numerical Simulation for Determination of Temperature Field and Residual Stress of Stainless Steel Butt Joints with and without Clamping, *Vietnam Journal of Science and Technology* **60** (4) (2022) 713-725.
10. Ngo Le Thong - Fusion electric welding technology - Volume 1: Theoretical foundations, Hanoi Science and Technology Publishing House, 2007 (in Vietnamese).
11. John A. Goldak, Mehdi Akhlaghi - *Computational welding mechanics*, Springer, 2005.
12. Diogo F. Almeida, Rui F. Martin, João B. Cardoso - Numerical simulation of residual stresses induced by TIG butt-welding of thin plates made of AISI 316L stainless steel, 2nd International Conference on Structural Integrity, Portugal, ICSI 2017, *Procedia Structure Integrity* **5** (2017) 633-639.
13. Abburi Venkata K., Truman C. E., Wimporoy R.C., Pirling T. - Numerical simulation of three-pass TIG welding using finite element method with validation from measurements, *International Journal of Pressure Vessels and Piping* **164** (2018) 68-79, <https://doi.org/10.1016/j.ijpvp.2017.05.014>.
14. Etienne Bonnaud, Jens Gunnars - Recommended residual stress profiles for stainless steel pipe welds, Report number: 2016:39, ISSN: 2000-0456, 2016.
15. Damian Kotecki, Frank Armao - *Stainless Steels – Welding Guide*, Lincoln Electric Company, 2003.